

Flavor and Energy Dependence of Chemical Freeze-out Temperatures in Relativistic Heavy Ion Collisions from RHIC-BES to LHC Energies

Fernando Antonio Flor,^{*} Gabrielle Olinger,[†] and René Bellwied[‡]
Department of Physics, University of Houston, Houston, Texas 77204, USA
(Dated: October 1, 2020)

We present calculations of the chemical freeze-out temperature (T_{ch}) based on particle yields from STAR and ALICE measured at collision energies ranging from $\sqrt{s_{\text{NN}}} = 11.5$ GeV to 5.02 TeV. Employing the Grand Canonical Ensemble approach using the Thermal-FIST Hadron Resonance Gas model package, we show evidence for a flavor-dependent chemical freeze-out in the crossover region of the QCD phase diagram. At a vanishing baryochemical potential, we calculate light and strange flavor freeze-out temperatures $T_{\text{L}} = 150.2 \pm 2.6$ MeV and $T_{\text{S}} = 165.1 \pm 2.7$ MeV, respectively.

I. INTRODUCTION

In depth determinations of a pseudo-critical temperature based on continuum extrapolations of temperature dependence of the chiral susceptibilities on the lattice, in comparison to calculations using Statistical Hadronization Models (SHM) using particle yields from experiments at the Relativistic Heavy Ion Collider (RHIC) and the Large Hadron Collider (LHC), indicate that chemical freeze-out and hadronization coincide near the phase boundary in the Quantum Chromodynamics (QCD) phase diagram [1–5]. Whether this transition from quark to hadron degrees of freedom occurs at a uniform temperature for all quark flavors remains a question of interest.

SHMs have been successful in adequately reproducing hadronic particle abundances over nine orders of magnitude in high energy collisions of heavy ions over a wide range in energy [6, 7]. In these calculations, assuming a thermally equilibrated system, experimental particle yields in relativistic heavy ion collisions serve as an anchor for the determination of common freeze-out parameters in the QCD phase diagram – namely, the baryochemical potential (μ_{B}) and the chemical freeze-out temperature (T_{ch}). The resulting parameters can also be compared with independently obtained results from either lattice QCD based susceptibility calculations of conserved quantum numbers or measurements of higher order fluctuations of net-particle distributions.

II. SEQUENTIAL FLAVOR FREEZE-OUT

Continuum extrapolated susceptibility calculations of single flavor quantum numbers on the lattice [8, 9] have shown a difference in the determined freeze-out temperatures between flavors in the crossover region of the QCD

phase diagram. This effect is likely due to the difference in the bare quark masses which is not negligible in a thermally equilibrated deconfined system near the phase boundary. In particular, a comparison of the flavor specific susceptibility ratios χ_4/χ_2 , suggested as an observable for directly determining freeze-out temperatures [10], show a deviation of the lattice and Hadron Resonance Gas (HRG) model calculations coinciding at the peaks of the lattice data, which occur at flavor specific temperatures differing by 15–20 MeV from light to strange quarks [9]. Net-particle fluctuation measurements by the STAR collaboration have also shown comparable temperature differences between the light and strange mesons [11, 12].

Thermal fits to experimental data via SHMs have shown similar results, depicting a difference in the freeze-out temperatures between flavors in the crossover region. The STAR Collaboration recently published the dependence of their thermal fits to the yields on the particle species included in the fit rendering a freeze-out temperature about 10 – 15 MeV lower for a fit pions, kaons and protons than a common freeze-out temperature extracted from fits to yields of all measured particle species [13]. Moreover, it has been shown that assuming two distinct freeze-out temperatures improves the overall fit to ALICE data. Thus, a point of interest arises when comparing the extracted freeze-out parameters obtained using different sets of particles in the SHM calculation. A first study of this approach was performed in Ref. [14].

III. MODEL AND DATA PREPARATION

The entirety of our analysis was performed using the open source Thermal FIST (The FIST) thermal model package [15]. Without loss of generality, The FIST is a user-friendly package within the family of HRG Models. Although there exists a wide range of options for the HRG model within The FIST framework, we restricted our analysis to the default – namely, modeling an ideal non-interacting gas of hadrons and resonances within a Grand Canonical Ensemble (GCE).

^{*}faffor@uh.edu

[†]gdolinger@uh.edu

[‡]bellwied@uh.edu

All our calculations used the PDG2016+ hadronic spectrum [16] as the HRG input list, including a total of 783 states (i.e. *, **, *** and **** states from the 2016 Particle Data Group Data Book [17]). Deviations of the HRG calculations from the lattice curves of flavor specific susceptibilities at specific temperatures in the crossover region may be affected by the inclusion of certain states [18–20], thus a realistic determination of the underlying hadronic spectrum is key to this study. The PDG2016+ hadronic spectrum has been shown to be an optimized compromise between too few (found) and too many (from a simple Quark Model) excited states when compared to a large number of lattice QCD predictions [16].

Yield data for π^+ , π^- , K^+ , K^- , p , \bar{p} , Λ , $\bar{\Lambda}$, Ξ^- , $\bar{\Xi}^+$, Ω^- , $\bar{\Omega}^+$, K_S^0 , and ϕ for ALICE PbPb collisions at $\sqrt{s_{NN}} = 2.76$ TeV [21–24] and preliminary results at 5.02 TeV [25] in the 0 - 10% centrality class, as well as STAR AuAu collisions at $\sqrt{s_{NN}} = 11.5, 19.6, 27.0, 39.0, 62.4$ and 200 GeV [13, 26–30] were used. We excluded AuAu collisions at $\sqrt{s_{NN}} = 7.7$ GeV due to the wider centrality binning of the data, particularly for multi-strange baryons.

For the sake of brevity, we introduced a shorthand notation when naming our fits with (anti)particle species (e.g. Ω refers to both Ω^- and $\bar{\Omega}^+$, etc.). This shorthand is used for the remainder of this letter.

(Anti)proton yields for the STAR data in Refs. [13, 28, 29] are all inclusive. In order to correct for weak-decay feed-down contributions from $(\bar{\Lambda})\Lambda$, we interpolated the contributions to (anti)proton yields based on the method suggested in Ref. [31]. Table I summarizes our interpolation results. The contribution from $(\bar{\Lambda})\Lambda$ to (anti)proton yields are labeled as δ . These δ values were subtracted from unity and multiplied by their respective (anti)proton yields. The resulting (anti)proton yields were then used for the entirety of this analysis. This procedure should be considered an upper limit for the feed-down contribution since the experiment imposes an, albeit loose, primary vertex cut on the $(\bar{\Lambda})\Lambda$ decay daughter candidates. These percentages are in general agreement with estimates in the aforementioned STAR papers, though.

TABLE I: Interpolation results from methods used in Ref. [31] for weak-decay feed-down contributions to (anti)proton yields at STAR AuAu Collisions from $\sqrt{s_{NN}} = 11.5$ to 200 GeV.

$\sqrt{s_{NN}}$ (GeV)	Proton δ	Anti-Proton δ
11.5	23.00%	48.00%
19.6	27.50%	44.00%
27.0	29.50%	41.50%
39.0	31.00%	40.00%
64.2	32.00%	38.50%
200	34.00%	36.50%

All our thermal fits were performed with T_{ch} (MeV) and

V (fm^3) as free parameters, setting γ_s and γ_q to unity. Our analysis focused on varying the particle species included in the fit. The particle species included in our temperature fits were $\pi K p$ (light), $\pi K p \Lambda \Xi \Omega K_S^0 \phi$ (all) and $K \Lambda \Xi \Omega K_S^0 \phi$ (strange), respectively. The inclusion of the kaons in the light fit was done in order to avoid too few degrees of freedom in the fit and has no effect on the extracted freeze-out temperature, since the kaon yield is rather insensitive to the temperature, as was also shown previously in Ref. [32]. For the two ALICE energies, we let $\mu_B = 0$. For all fits to STAR AuAu data, we let μ_B be a free parameter in the fits to also gauge its sensitivity to the flavor-specific fits.

IV. RESULTS AND DISCUSSION

We extracted freeze-out parameters, T_{ch} and V , for the full ($\pi K p \Lambda \Xi \Omega K_S^0 \phi$), light ($\pi K p$), and strange ($K \Lambda \Xi \Omega K_S^0 \phi$) particle thermal fits. Figure 1 shows T_{ch} from the full fits as a function of μ_B . The magenta line represents the spline fit function with three nodes (PbPb at $\sqrt{s_{NN}} = 5.02$ TeV and AuAu at $\sqrt{s_{NN}} = 27.0$ and 19.6 GeV) to the freeze-out parameters. The magenta band represents the residual to the spline fit and is determined by the mean square error of the spline function.

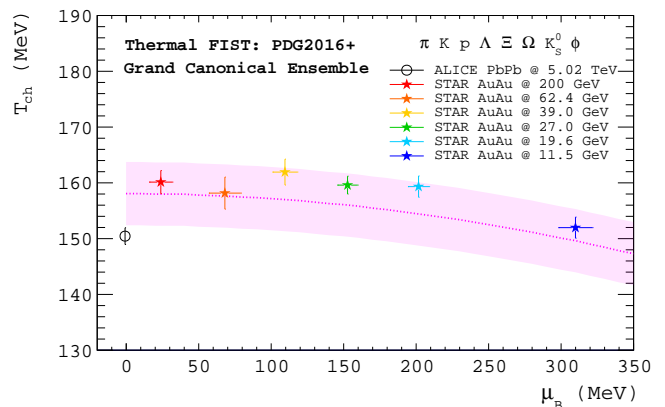


FIG. 1: Full GCE fits to STAR and ALICE data measured at collision energies ranging from $\sqrt{s_{NN}} = 11.5$ GeV to 5.02 TeV (0 - 10%) using The FIST with the PDG2016+ hadronic spectrum. Magenta bands shows a spline fit to the points.

Figure 2 shows T_{ch} from the light and strange fit as a function of μ_B ; both fits are compared to Lattice QCD calculations in Ref. [1]. Each flavor dependent spline fit and error band was determined in the same manner as in Figure 1. The width of the lattice curve is based on the width (σ) of the chiral susceptibility [1].

Detailed fit results for each energy including V and χ^2/dof , are shown in Table II. Generally the separation into light and strange particles improves the quality of the fits by at least a factor two at all energies.

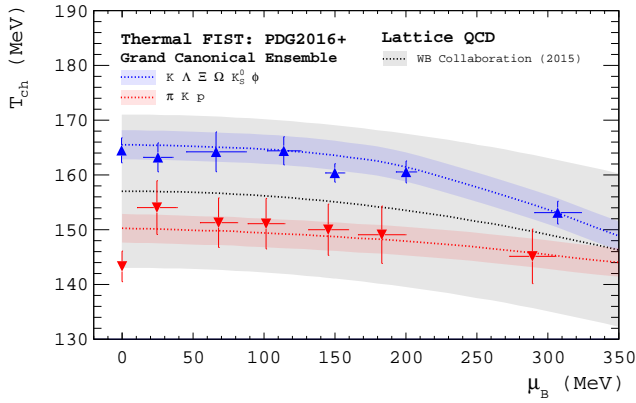


FIG. 2: *Strange* (blue points) and *light* (red points) GCE fits to STAR and ALICE data measured at collision energies ranging from $\sqrt{s_{NN}} = 11.5$ GeV to 5.02 TeV (0 - 10%) via The FIST using the PDG2016+ hadronic spectrum.

In Figure 2, the light and strange fits consistently fall within the lattice QCD crossover width as long as that width is defined by the pseudo-critical temperature of all possible order parameters. Our flavor-dependent fits agree with the calculated freeze-out temperatures from net-proton, net-charge and net-kaon fluctuations up to $\mu_B \simeq 150$ MeV [12, 33]. T_{ch} remains constant with increasing μ_B until $\mu_B \simeq 100$ MeV, where the strange and light fit begin to approach. The two fits converge within errors at $\mu_B \simeq 300$ MeV; therefore, we propose that a separate treatment of strange and light particles might not be meaningful at $\mu_B \geq 300$ MeV. The convergence of the two flavor-dependent temperatures is expected in the vicinity of a critical point in the QCD phase diagram.

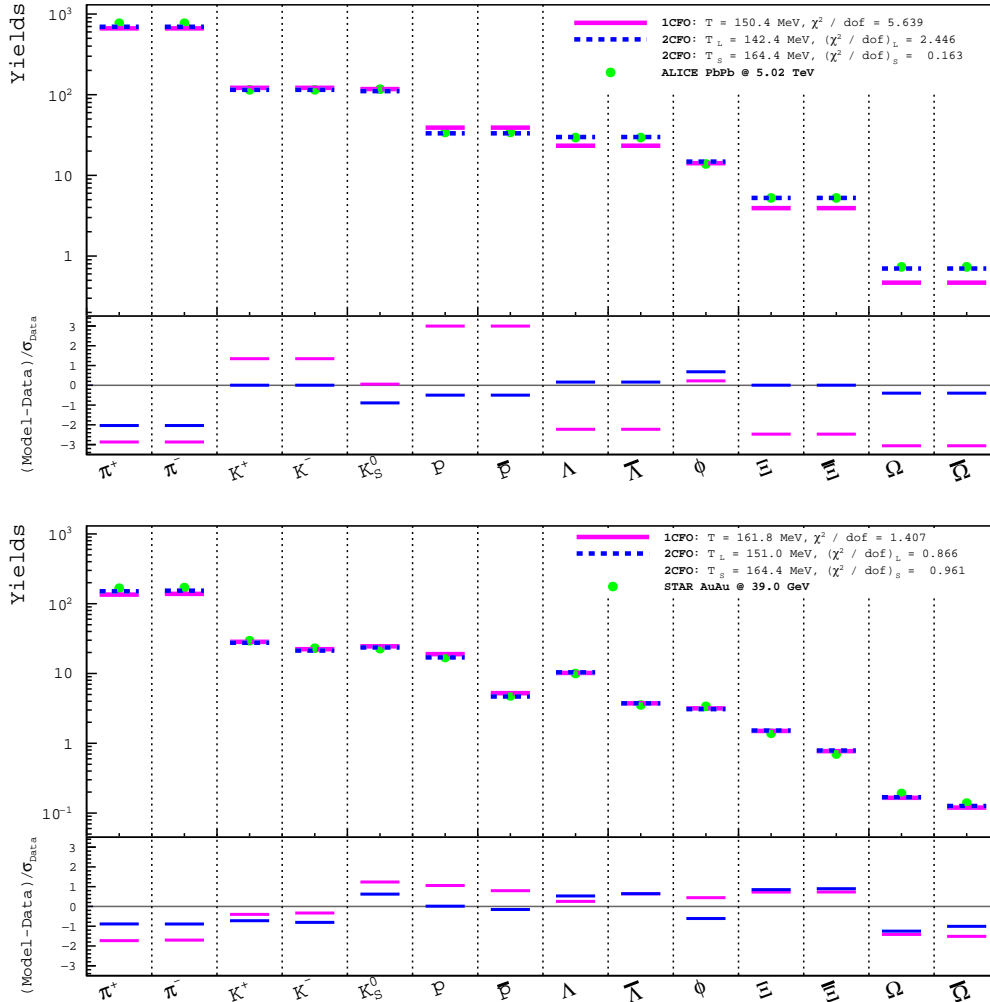


FIG. 3: Top and bottom panels show GCE fits to ALICE PbPb at $\sqrt{s_{NN}} = 5.02$ TeV (0 - 10%) and STAR AuAu at $\sqrt{s_{NN}} = 39.0$ GeV (0 - 10%), respectively, via The FIST using the PDG2016+ hadronic spectrum. Single temperature (1CFO) yield calculations are shown in magenta. Two temperature (2CFO) yield calculations are shown in dashed blue lines. Experimental values [25, 26] are shown in green.

TABLE II: The FIST Grand Canonical Ensemble Yield Fits via the PDG2016+ hadronic spectrum for collision energies ranging from $\sqrt{s_{\text{NN}}} = 11.5$ to 200 GeV. The top, middle and bottom sections show the full ($\pi K p \Lambda \Xi \Omega K_S^0 \phi$), light ($\pi K p$), and strange ($K \Lambda \Xi \Omega K_S^0 \phi$) particle fits, respectively. For all fits, μ_B , T_{ch} , and V were used as free parameters.

$\pi K p \Lambda \Xi \Omega K_S^0 \phi$				
$\sqrt{s_{\text{NN}}}$ (GeV)	μ_B (MeV)	T_{ch} (MeV)	V ($f m^3$)	χ^2/dof
5020	0.0	150.4 ± 1.50	6238.8 ± 538.8	78.9/12
2760	0.0	149.6 ± 1.76	5764.4 ± 635.8	23.4/12
200	25.0 ± 7.94	160.0 ± 2.07	1596.3 ± 198.3	23.3/10
62.4	68.4 ± 11.0	158.1 ± 2.87	1151.7 ± 178.2	41.0/11
39	110.3 ± 8.51	161.8 ± 2.32	751.6 ± 103.0	15.5/11
27	154.2 ± 6.92	159.4 ± 1.60	741.8 ± 70.4	12.8/11
19.6	202.8 ± 7.29	159.3 ± 1.91	643.2 ± 72.6	15.2/11
11.5	310.7 ± 11.7	151.8 ± 1.89	649.4 ± 78.8	15.9/11
$\pi K p$				
$\sqrt{s_{\text{NN}}}$ (GeV)	μ_B (MeV)	T_{ch} (MeV)	V ($f m^3$)	χ^2/dof
5020	0.0	142.4 ± 1.70	9371.6 ± 902.1	14.6/4
2760	0.0	143.2 ± 2.79	8031.7 ± 1263.0	5.65/4
200	24.5 ± 14.0	153.9 ± 4.91	2210.0 ± 553.4	3.10/3
62.4	67.8 ± 13.1	151.2 ± 4.53	1721.7 ± 394.5	7.79/3
39	101.4 ± 12.9	151.0 ± 4.61	1368.8 ± 338.9	2.60/3
27	145.3 ± 14.0	149.9 ± 4.68	1333.3 ± 336.8	2.79/3
19.6	182.9 ± 16.7	149.0 ± 5.24	1186.1 ± 341.5	7.66/3
11.5	289.4 ± 16.2	145.0 ± 4.98	1074.8 ± 300.1	2.67/3
$K \Lambda \Xi \Omega K_S^0 \phi$				
$\sqrt{s_{\text{NN}}}$ (GeV)	μ_B (MeV)	T_{ch} (MeV)	V ($f m^3$)	χ^2/dof
5020	0.0	164.4 ± 2.28	3086.8 ± 366.7	1.58/8
2760	0.0	153.9 ± 2.30	4389.7 ± 640.8	10.5/8
200	25.7 ± 10.3	163.2 ± 2.64	1287.5 ± 208.8	17.3/6
62.4	66.7 ± 21.0	164.2 ± 3.63	784.5 ± 152.2	21.4/7
39	116.0 ± 11.7	164.4 ± 2.57	643.6 ± 97.7	6.73/7
27	156.0 ± 7.88	160.4 ± 1.68	695.0 ± 69.3	3.55/7
19.6	206.5 ± 8.30	160.7 ± 2.00	585.2 ± 69.3	3.87/7
11.5	321.0 ± 14.7	153.4 ± 2.08	574.8 ± 77.2	5.36/7

The greatest difference between the two temperatures is seen at the highest energy, namely the ALICE top energy. To address the impact of a flavor dependent freeze-out on the particle abundances, we calculated yields for the full particle set ($\pi K p \Lambda \Xi \Omega K_S^0 \phi$) for ALICE PbPb 5.02 TeV with a one chemical freeze-out (1CFO) approach and compared them with yields calculated for light ($\pi K p$) and strange ($K \Lambda \Xi \Omega K_S^0 \phi$) particles separately with a two chemical freeze-out (2CFO) approach. We fixed the temperature(s) and volume(s) to the T_{ch} and V values shown in Table II for $\sqrt{s_{\text{NN}}} = 5020$ GeV. In the 1CFO approach, we calculated yields using a temperature of 150.4 MeV. In the 2CFO approach, our light and strange particle yield calculations were done with temperatures fixed to 142.4 MeV and 164.4 MeV, respectively. We note that our 1CFO temperature differs from the value quoted by ALICE, which is based on the Heidelberg-GSI model, by about 4 MeV, most likely due to the difference in the

hadronic input spectrum [25].

Figure 3 shows this comparison of 1CFO and 2CFO approaches for full datasets at two exemplary energies, namely the preliminary 5.02 TeV central PbPb data from ALICE and the 39.0 GeV central AuAu data from STAR. The deviations of each yield calculation from the experimental value are shown at the bottom of each plot. We observe that the 2CFO approach provides an excellent and much improved description of the experimental data; rendering yields within one standard deviation of the experimental measurements for most particle species. The 2CFO treatment all but eliminates the tension between light and strange baryons, the so-called proton anomaly, seen in the 1CFO approach. It should also be noted that alternative methods to treat interactions in the SHM via the S-matrix approach [34] impact in particular the proton yields and improve the performance of the 1CFO method in the Heidelberg-GSI fits [7].

V. CONCLUSION

We presented calculations of the chemical freeze-out temperature (T_{ch}) based on particle yields from STAR and ALICE measured at collision energies ranging from $\sqrt{s_{\text{NN}}} = 11.5$ GeV to 5.02 TeV. Based on a splined fit to our thermal fit parameters at all energies, we calculated a light flavor freeze-out temperature $T_{\text{L}} = 150.2 \pm 2.6$ MeV and a strange flavor freeze-out temperature $T_{\text{S}} = 165.1 \pm 2.7$ MeV at vanishing μ_{B} , employing the GCE approach within the framework of the The FIST HRG model package. We showed evidence for flavor-dependent chemical freeze-out temperatures in the crossover region of the QCD phase diagram, which start to converge above $\mu_{\text{B}} \simeq 300$ MeV. We employed the flavor-dependent two temperature approach via The FIST to successfully

model and reproduce experimental yields at top ALICE energies. Thus, at the highest energies at RHIC and the LHC a separation of the hadronization temperature of light and strange particles seems likely. Furthermore, our results suggest the existence of a critical point in the QCD phase diagram above $\mu_{\text{B}} \simeq 300$ MeV and a temperature below $T_{\text{ch}} \simeq 150$ MeV.

VI. ACKNOWLEDGMENTS

The authors acknowledge edifying discussions with Volodymyr Vovchenko, Claudia Ratti, Paolo Parotto, Jamie Stafford, Livio Bianchi and Boris Hippolyte. This work was supported by the DOE grant DEFG02-07ER4152.

-
- [1] R. Bellwied, S. Borsányi, Z. Fodor, J. Günther, S. Katz, C. Ratti, and K. Szabó, *Physics Letters B* **751**, 559 (2015).
 - [2] S. Borsányi, Z. Fodor, C. Hoelbling, S. D. Katz, S. Krieg, C. Ratti, and K. K. Szabó, *Journal of High Energy Physics* **2010**, 73 (2010).
 - [3] S. Borsányi, Z. Fodor, C. Hoelbling, S. D. Katz, S. Krieg, and K. K. Szabó, *Physics Letters B* **730**, 99 (2014).
 - [4] A. Bazavov *et al.* (HotQCD Collaboration), *Phys. Rev. D* **90**, 094503 (2014).
 - [5] J. Stachel, A. Andronic, P. Braun-Munzinger, and K. Redlich, *Journal of Physics: Conference Series* **509**, 012019 (2014).
 - [6] J. Cleymans and K. Redlich, *Phys. Rev. Lett.* **81**, 5284 (1998).
 - [7] A. Andronic, P. Braun-Munzinger, K. Redlich, and J. Stachel, *Nature* **561**, 321 (2018).
 - [8] C. Ratti, R. Bellwied, M. Cristoforetti, and M. Barbaro, *Phys. Rev. D* **85**, 014004 (2012).
 - [9] R. Bellwied, S. Borsanyi, Z. Fodor, S. D. Katz, and C. Ratti, *Phys. Rev. Lett.* **111**, 202302 (2013).
 - [10] F. Karsch, *Central European Journal of Physics* **10**, 1234 (2012).
 - [11] L. Adamczyk *et al.* (STAR Collaboration), *Phys. Rev. Lett.* **112**, 032302 (2014).
 - [12] R. Bellwied, J. Noronha-Hostler, P. Parotto, I. Portillo Vazquez, C. Ratti, and J. M. Stafford, *Phys. Rev. C* **99**, 034912 (2019).
 - [13] L. Adamczyk *et al.* (STAR Collaboration), *Phys. Rev. C* **96**, 044904 (2017).
 - [14] S. Chatterjee, A. K. Dash, and B. Mohanty, *Journal of Physics G: Nuclear and Particle Physics* **44**, 105106 (2017).
 - [15] V. Vovchenko and H. Stoecker, *Computer Physics Communications* **244**, 295 (2019).
 - [16] P. Alba, R. Bellwied, S. Borsányi, Z. Fodor, J. Günther, S. D. Katz, V. Mantovani Sarti, J. Noronha-Hostler, P. Parotto, A. Pasztor, I. P. Vazquez, and C. Ratti, *Phys. Rev. D* **96**, 034517 (2017).
 - [17] C. Patrignani *et al.* (Particle Data Group), *Chin. Phys.* **C40**, 100001 (2016).
 - [18] J. Noronha-Hostler and C. Greiner, *Nuclear Physics A* **931**, 1108 (2014).
 - [19] P. Alba, V. M. Sarti, J. Noronha-Hostler, P. Parotto, I. Portillo-Vazquez, C. Ratti, and J. M. Stafford, *Phys. Rev. C* **101**, 054905 (2020).
 - [20] A. Bazavov, H.-T. Ding, P. Hegde, O. Kaczmarek, F. Karsch, E. Laermann, Y. Maezawa, S. Mukherjee, H. Ohno, P. Petreczky, C. Schmidt, S. Sharma, W. Soeldner, and M. Wagner, *Phys. Rev. Lett.* **113**, 072001 (2014).
 - [21] B. Abelev *et al.* (ALICE Collaboration), *Phys. Rev. C* **88**, 044910 (2013).
 - [22] B. Abelev *et al.* (ALICE Collaboration), *Phys. Rev. Lett.* **111**, 222301 (2013).
 - [23] B. Abelev *et al.* (ALICE Collaboration), *Phys. Rev. C* **91**, 024609 (2015).
 - [24] B. Abelev *et al.* (ALICE Collaboration), *Physics Letters B* **728**, 216 (2014).
 - [25] F. Bellini (ALICE Collaboration), *Nuclear Physics A* **982**, 427 (2019).
 - [26] J. Adam *et al.* (STAR Collaboration), *Phys. Rev. C* **102**, 034909 (2020).
 - [27] B. I. Abelev *et al.* (STAR Collaboration), *Phys. Rev. C* **79**, 034909 (2009).
 - [28] M. M. Aggarwal *et al.* (STAR Collaboration), *Phys. Rev. C* **83**, 024901 (2011).
 - [29] G. Agakishiev *et al.* (STAR Collaboration), *Phys. Rev. Lett.* **108**, 072301 (2012).
 - [30] J. Adams *et al.* (STAR Collaboration), *Phys. Rev. Lett.* **98**, 062301 (2007).
 - [31] A. Andronic, P. Braun-Munzinger, and J. Stachel, *Nuclear Physics A* **772**, 167 (2006).
 - [32] D. Magestro, *Journal of Physics G: Nuclear and Particle Physics* **28**, 1745 (2002).
 - [33] P. Alba, W. Alberico, R. Bellwied, M. Bluhm, V. M.

- Sarti, M. Nahrgang, and C. Ratti, *Physics Letters B* **738**, 305 (2014).
- [34] A. Andronic, P. Braun-Munzinger, B. Friman, P. M. Lo, K. Redlich, and J. Stachel, *Phys. Lett.* **B792**, 304 (2019).